

Space-frequency coded orthogonal signal-division multiplexing over underwater acoustic channels

Jing Han^{a)} and Wentao Shi

School of Marine Science and Technology, Northwestern Polytechnical University,
Xi'an 710072, China
hanj@nwpu.edu.cn, swt@nwpu.edu.cn

Geert Leus

Faculty of Electrical Engineering, Mathematics and Computer Science,
Delft University of Technology, 2826 CD Delft, The Netherlands
g.j.t.leus@tudelft.nl

Abstract: Orthogonal signal-division multiplexing (OSDM) is a newly emerged modulation scheme which provides a generalized framework unifying conventional orthogonal frequency-division multiplexing (OFDM) and single-carrier frequency domain equalization. In this letter, a space-frequency block coding (SFBC) scheme based on OSDM is proposed for time-varying underwater acoustic channels. The receiver processing includes Doppler compensation, channel estimation, space-frequency decoding, and equalization. Simulation and experimental results demonstrate its superiority over the existing SFBC-OFDM counterpart.

© 2017 Acoustical Society of America

[LMZ]

Date Received: February 16, 2017 Date Accepted: May 3, 2017

1. Introduction

Recently, orthogonal frequency-division multiplexing (OFDM) has been widely investigated for underwater acoustic (UWA) communications, thanks to its ability to mitigate intersymbol interference with low-complexity frequency-domain equalization.¹ However, it is well known that OFDM cannot ensure reliable communication because each data symbol is transmitted over a single flat subchannel that may undergo fading. To improve its robustness, channel coding,² receive diversity,^{3,4} and transmit diversity^{5,6} are usually adopted. Among these techniques, transmit diversity has the advantage of collecting diversity gain without significantly sacrificing bandwidth efficiency or increasing the size of the receiver. So far, as two typical examples, space-time block coding⁵ and space-frequency block coding (SFBC)⁶ have been used in underwater OFDM communications, where the latter offers a better resilience to channel time variations since its Alamouti structure is confined within a single block.⁶

In this letter, we consider a newly emerged modulation, namely orthogonal signal-division multiplexing (OSDM), based on which an SFBC-OSDM scheme is proposed to establish reliable communication over time-varying UWA channels. This scheme is an important extension of our previous work for time-invariant channels in Ref. 7. By further introducing Doppler compensation and channel estimation based on null symbols and precoded pilot vectors, it can achieve a better symbol-error-rate (SER) performance in comparison with the existing SFBC-OFDM system. Both numerical simulation and field experimental results are presented to validate the enhanced performance of the proposed scheme.

Notation: $(\cdot)^*$ stands for conjugate, $(\cdot)^T$ for transpose, $(\cdot)^H$ for Hermitian transpose, $(\cdot)^\dagger$ for Moore-Penrose pseudo-inverse, and $|\cdot|$ for Euclidean norm. Furthermore, $[\mathbf{x}]_{m:n}$ indicates the subvector of \mathbf{x} from entry m to n . We define $\text{diag}\{\mathbf{x}\}$ as a diagonal matrix created from the vector \mathbf{x} , and $\text{Diag}\{\mathbf{A}_1, \dots, \mathbf{A}_M\}$ as a block diagonal matrix created with the submatrices $\mathbf{A}_1, \dots, \mathbf{A}_M$. Moreover, \mathbf{F}_M and \mathbf{I}_M are the $M \times M$ unitary discrete Fourier transform (DFT) and identity matrix, respectively; \mathbf{P}_M is the permutation matrix satisfying $[\mathbf{P}_M \mathbf{x}]_m = [\mathbf{x}]_{(-m) \bmod M}$. Also, $\mathbf{0}_M$ denotes the $M \times 1$ all-zero vector; $\mathbf{f}_M(m)$ and $\mathbf{e}_M(m)$ are the m th columns of \mathbf{F}_M and \mathbf{I}_M , respectively.

2. OSDM signal model

OSDM is a generalized modulation scheme which connects OFDM and single-carrier frequency domain equalization in a unified framework. It shares a similar signal

^{a)} Author to whom correspondence should be addressed.

structure as vector OFDM first proposed in Ref. 8, and was recently used for UWA communications in Refs. 9 and 10. In this section, for a better understanding, we will start from a review of the simple time-invariant single-input single-output (SISO) configuration and then move on to the SFBC case over time-varying UWA channels.

2.1 SISO-OSDM over time-invariant channels

Assume that $\mathbf{x} = [x_0, x_1, \dots, x_{K-1}]^T$ is the data block of $K = MN$ symbols to be modulated. Unlike OFDM modulation which treats \mathbf{x} as a whole, the OSDM scheme further divides it into N symbol vectors of length M , i.e., $\mathbf{x} = [\mathbf{x}_0^T, \mathbf{x}_1^T, \dots, \mathbf{x}_{N-1}^T]^T$, where $\mathbf{x}_n = [x_{nM}, x_{nM+1}, \dots, x_{nM+M-1}]^T$ for $n=0, \dots, N-1$. Moreover, instead of performing a single K -point inverse DFT as in the OFDM system, the data block is modulated by M inverse DFTs of length N in the OSDM system, which yields

$$\mathbf{s} = (\mathbf{F}_N^H \otimes \mathbf{I}_M)\mathbf{x}, \quad (1)$$

where \otimes denotes the Kronecker product. Then, the signal block \mathbf{s} is appended with a cyclic prefix (CP), upconverted, and transmitted over a channel. It is easy to show that, by shortening the DFT size from K to N , OSDM can produce a lower peak-to-average power ratio than conventional OFDM.

At the receiver, after downconverting and removing the CP, OSDM demodulation takes the form

$$\mathbf{y} = (\mathbf{F}_N \otimes \mathbf{I}_M)\mathbf{r}, \quad (2)$$

where \mathbf{r} and \mathbf{y} are the $K \times 1$ baseband received and demodulated blocks, respectively. The demodulated block is also partitioned into vectors, i.e., $\mathbf{y} = [\mathbf{y}_0^T, \mathbf{y}_1^T, \dots, \mathbf{y}_{N-1}^T]^T$ with $\mathbf{y}_n = [y_{nM}, y_{nM+1}, \dots, y_{nM+M-1}]^T$. For simplicity, we first assume the channel to be time-invariant with length- $(L+1)$ impulse response $\mathbf{h} = [h_0, h_1, \dots, h_L]^T$. In this case, decoupled detection among vectors can be achieved, since we have⁸

$$\mathbf{y}_n = [\mathbf{f}_N^T(n) \otimes \mathbf{I}_M]\mathbf{r} = \mathbf{U}_n^H \mathbf{H}_n \mathbf{U}_n \mathbf{x}_n + \mathbf{z}_n, \quad n = 0, \dots, N-1, \quad (3)$$

where $\mathbf{H}_n = \text{diag}\{[H_n, H_{n+N}, \dots, H_{n+(M-1)N}]\}$ is the decimated frequency response (DFR) submatrix with entries $H_{n+mN} = \sum_{l=0}^L h_l e^{-j2\pi l(n+mN)/K}$ for $m=0, \dots, M-1$, $\mathbf{U}_n = \mathbf{F}_M \mathbf{\Lambda}_n$ with $\mathbf{\Lambda}_n = \text{diag}\{[1, e^{-j(2\pi n/K)}, \dots, e^{-j2\pi(M-1)n/K}]\}$, and \mathbf{z}_n is the noise term.

2.2 SFBC-OSDM over time-varying UWA channels

We now turn to the SFBC-OSDM scenario with two transmit and one receive element. Moreover, time-varying UWA channels are also taken into account. We here assume that the two transmit elements are co-located and the time variation over all channel paths can be simply modeled by a common Doppler scaling factor. It has been clarified that, under this kind of assumption, the time variation in the received signal after front-end resampling approximately reduces to a carrier frequency offset (CFO).³ Therefore, the Doppler distortion in wideband signals of UWA communications can be efficiently mitigated by a narrowband operation of CFO compensation. In this letter, a similar strategy is adopted for the proposed SFBC-OSDM system.

Specifically, the demodulation in this case needs to be preceded by CFO compensation. Based on Eq. (3), we introduce a frequency parameter ϵ and define $\mathbf{y}_n(\epsilon) = [\mathbf{f}_N^T(n) \otimes \mathbf{I}_M]\mathbf{\Gamma}^H(\epsilon)\mathbf{r}$, where $\mathbf{\Gamma}(\epsilon) = \text{diag}\{[1, e^{j2\pi\epsilon}, \dots, e^{j2\pi(K-1)\epsilon}]\}$. Also, let ϵ_0 and $\hat{\epsilon}_0$ be the post-resampling CFO and its estimate. The demodulated vector of the SFBC-OSDM system is then denoted as $\mathbf{y}_n = \mathbf{y}_n(\hat{\epsilon}_0)$ for notational simplicity. Compared to the SISO-OSDM case shown in Eq. (3), when the channel time variations are completely removed, i.e., $\hat{\epsilon}_0 = \epsilon_0$, it now has the form

$$\mathbf{y}_n = \mathbf{U}_n^H \mathbf{H}_n^{(1)} \mathbf{U}_n \bar{\mathbf{x}}_n^{(1)} + \mathbf{U}_n^H \mathbf{H}_n^{(2)} \mathbf{U}_n \bar{\mathbf{x}}_n^{(2)} + \mathbf{z}_n, \quad n = 0, \dots, N-1, \quad (4)$$

where $\mathbf{H}_n^{(\mu)}$ and $\bar{\mathbf{x}}_n^{(\mu)}$ are the DFR submatrix and the space-frequency coded vector corresponding to the transmit element $\mu \in \{1, 2\}$. On the other hand, in the presence of channel time variations, unlike inter-carrier interference in OFDM, inter-vector interference arises in OSDM. In Sec. 3, we will explain in detail the space-frequency coding scheme, i.e., how to design $\bar{\mathbf{x}}_n^{(\mu)}$, and the channel estimation method, i.e., how to estimate ϵ_0 and $\mathbf{H}_n^{(\mu)}$.

3. Proposed SFBC-OSDM scheme

In our scheme, space-frequency coding and channel estimation are performed on pairs of symbol vectors. Similar as in Sec. 2, let us consider a SFBC-OSDM block consisting of N symbol vectors of length M . Here, each two consecutive symbol vectors are

further grouped into a vector pair (VP), and all $P = N/2$ VPs are divided into two categories: (1) Q pilot VPs for channel estimation, and (2) the remaining $P - Q$ data VPs with space-frequency coding. We denote the index sets of pilot and data VPs by \mathcal{N}_p and \mathcal{N}_d , respectively. The corresponding signal structure and receiver processing for these two kinds of VPs are presented next.

3.1 Space-frequency coding with data VPs

For each data VP $p \in \mathcal{N}_d$, a phase-rotation-based scheme has been proposed in our previous work for time-invariant channels,⁷ where the space-frequency encoder generates the coded vectors as

$$\begin{bmatrix} \bar{\mathbf{x}}_{2p}^{(1)} & \bar{\mathbf{x}}_{2p+1}^{(1)} \\ \bar{\mathbf{x}}_{2p}^{(2)} & \bar{\mathbf{x}}_{2p+1}^{(2)} \end{bmatrix} = \begin{bmatrix} \Lambda_{2p}^H \mathbf{x}_{2p} & \Lambda_{2p+1}^H \mathbf{x}_{2p+1} \\ -\Lambda_{2p}^H \mathbf{P}_M \mathbf{x}_{2p+1}^* & \Lambda_{2p+1}^H \mathbf{P}_M \mathbf{x}_{2p}^* \end{bmatrix}. \quad (5)$$

Here, matrices Λ_{2p} and Λ_{2p+1} are employed for phase rotation. It can be seen that, if $M = 1$, Eq. (5) reduces to the conventional SFBC-OFDM scheme.

At the receiver, we define $\mathbf{X}_n = \mathbf{F}_M \mathbf{x}_n$, $\bar{\mathbf{Y}}_n = \mathbf{U}_n \mathbf{y}_n$, and $\bar{\mathbf{Z}}_n = \mathbf{U}_n \mathbf{z}_n$, and transform the demodulated vectors $\{\mathbf{y}_n\}$ in Eq. (4) to the frequency domain. By substituting Eq. (5) into Eq. (4), and assuming the DFR submatrices are constant between adjacent vectors, i.e., $\mathbf{H}_{2p}^{(\mu)} = \mathbf{H}_{2p+1}^{(\mu)}$, $\mu \in \{1, 2\}$, it can be derived that

$$\begin{bmatrix} \bar{\mathbf{Y}}_{2p} \\ \bar{\mathbf{Y}}_{2p+1}^* \end{bmatrix} = \begin{bmatrix} \mathbf{H}_{2p}^{(1)} & -\mathbf{H}_{2p}^{(2)} \\ \mathbf{H}_{2p}^{(2)*} & \mathbf{H}_{2p}^{(1)*} \end{bmatrix} \begin{bmatrix} \mathbf{X}_{2p} \\ \mathbf{X}_{2p+1}^* \end{bmatrix} + \begin{bmatrix} \bar{\mathbf{Z}}_{2p} \\ \bar{\mathbf{Z}}_{2p+1}^* \end{bmatrix}. \quad (6)$$

Then, the space-frequency decoding can be performed as

$$\begin{aligned} \begin{bmatrix} \tilde{\mathbf{Y}}_{2p} \\ \tilde{\mathbf{Y}}_{2p+1}^* \end{bmatrix} &= \begin{bmatrix} \mathbf{H}_{2p}^{(1)} & -\mathbf{H}_{2p}^{(2)} \\ \mathbf{H}_{2p}^{(2)*} & \mathbf{H}_{2p}^{(1)*} \end{bmatrix}^H \begin{bmatrix} \bar{\mathbf{Y}}_{2p} \\ \bar{\mathbf{Y}}_{2p+1}^* \end{bmatrix} \\ &= \begin{bmatrix} \tilde{\mathbf{H}}_{2p} & 0 \\ 0 & \tilde{\mathbf{H}}_{2p} \end{bmatrix} \begin{bmatrix} \mathbf{X}_{2p} \\ \mathbf{X}_{2p+1}^* \end{bmatrix} + \begin{bmatrix} \tilde{\mathbf{Z}}_{2p} \\ \tilde{\mathbf{Z}}_{2p+1}^* \end{bmatrix}, \end{aligned} \quad (7)$$

where $\tilde{\mathbf{H}}_{2p} = \mathbf{H}_{2p}^{(1)H} \mathbf{H}_{2p}^{(1)} + \mathbf{H}_{2p}^{(2)H} \mathbf{H}_{2p}^{(2)}$; $\tilde{\mathbf{Z}}_{2p}$ and $\tilde{\mathbf{Z}}_{2p+1}^*$ are noise terms. Therefore, decoupled detection can be achieved between symbol vectors $2p$ and $2p + 1$. We can finally obtain the frequency-domain equalization matrix in the minimum mean-square error sense as⁷

$$\mathbf{W}_{2p} = \mathbf{W}_{2p+1} = (\tilde{\mathbf{H}}_{2p} + \sigma_z^2 \mathbf{I}_M)^{-1}, \quad (8)$$

where σ_z^2 is the variance of the noise samples in \mathbf{z}_n .

3.2 Channel estimation with pilot VPs

Note that, in the derivations of Eqs. (6) and (7), the channel is assumed to be time-invariant and known to the receiver. However, for practical UWA applications, channel estimation and Doppler compensation have to be considered. To this end, two $MQ \times 1$ pilot sequences $\mathbf{d}^{(\mu)} = [d_0^{(\mu)}, d_1^{(\mu)}, \dots, d_{MQ-1}^{(\mu)}]^T$, $\mu = 1, 2$, are used. Also, I null symbols are located randomly in $\mathbf{d}^{(\mu)}$ at indices $k_1^{(\mu)}, \dots, k_I^{(\mu)}$ to estimate the post-resampling CFO, i.e., $\mathbf{E}^{(\mu)} \mathbf{d}^{(\mu)} = \mathbf{0}_I$, where $\mathbf{E}^{(\mu)} = [\mathbf{e}_{MQ}(k_1^{(\mu)}), \mathbf{e}_{MQ}(k_2^{(\mu)}), \dots, \mathbf{e}_{MQ}(k_I^{(\mu)})]^T$. For each pilot VP $p \in \mathcal{N}_p$, we perform precoding as follows:

$$\begin{bmatrix} \bar{\mathbf{x}}_{2p}^{(1)} & \bar{\mathbf{x}}_{2p+1}^{(1)} \\ \bar{\mathbf{x}}_{2p}^{(2)} & \bar{\mathbf{x}}_{2p+1}^{(2)} \end{bmatrix} = \begin{bmatrix} \mathbf{U}_{2p}^H \mathbf{x}_{2p} & \mathbf{0}_M \\ \mathbf{0}_M & \mathbf{U}_{2p+1}^H \mathbf{x}_{2p+1} \end{bmatrix}, \quad (9)$$

where \mathbf{x}_{2p} and \mathbf{x}_{2p+1} are segments in $\{\mathbf{d}^{(\mu)}\}$. Assuming $\mathcal{N}_p = \{p_1, p_2, \dots, p_Q\}$, we take $\mathbf{x}_{2p_q} = [\mathbf{d}^{(1)}]_{(q-1)M:qM-1}$ and $\mathbf{x}_{2p_q+1} = [\mathbf{d}^{(2)}]_{(q-1)M:qM-1}$ for $q = 1, 2, \dots, Q$. Note that, unlike

the Alamouti-like coding for the data VPs in Eq. (5), pilot VPs are here coded in an on-off way to facilitate decoupled channel estimation at the receiver.

We then define $\bar{\mathbf{Y}}_n(\epsilon) = \mathbf{U}_n \mathbf{y}_n(\epsilon)$. From Eqs. (4) and (9), it can be obtained that $\bar{\mathbf{Y}}_{2p}(\epsilon_0) = \mathbf{H}_{2p}^{(1)} \mathbf{x}_{2p} + \bar{\mathbf{Z}}_{2p}$ and $\bar{\mathbf{Y}}_{2p+1}(\epsilon_0) = \mathbf{H}_{2p+1}^{(2)} \mathbf{x}_{2p+1} + \bar{\mathbf{Z}}_{2p+1}$ for $p \in \mathcal{N}_p$. Furthermore, by stacking the even and odd pilot vectors, it yields

$$\bar{\mathbf{Y}}^{(1)}(\epsilon_0) = \text{Diag}\{\mathbf{H}_{2p_1}^{(1)}, \mathbf{H}_{2p_2}^{(1)}, \dots, \mathbf{H}_{2p_Q}^{(1)}\} \mathbf{d}^{(1)} + \bar{\mathbf{Z}}^{(1)}, \tag{10}$$

$$\bar{\mathbf{Y}}^{(2)}(\epsilon_0) = \text{Diag}\{\mathbf{H}_{2p_1+1}^{(2)}, \mathbf{H}_{2p_2+1}^{(2)}, \dots, \mathbf{H}_{2p_Q+1}^{(2)}\} \mathbf{d}^{(2)} + \bar{\mathbf{Z}}^{(2)}, \tag{11}$$

where we have defined that $\bar{\mathbf{Y}}^{(1)}(\epsilon) = [\bar{\mathbf{Y}}_{2p_1}^T(\epsilon), \bar{\mathbf{Y}}_{2p_2}^T(\epsilon), \dots, \bar{\mathbf{Y}}_{2p_Q}^T(\epsilon)]^T$ and $\bar{\mathbf{Y}}^{(2)}(\epsilon) = [\bar{\mathbf{Y}}_{2p_1+1}^T(\epsilon), \bar{\mathbf{Y}}_{2p_2+1}^T(\epsilon), \dots, \bar{\mathbf{Y}}_{2p_Q+1}^T(\epsilon)]^T$, while $\bar{\mathbf{Z}}^{(1)}$ and $\bar{\mathbf{Z}}^{(2)}$ are the corresponding noise terms. Now, similar as the method in Ref. 3, a CFO estimate $\hat{\epsilon}_0$ can be obtained by minimizing the overall energy on the null symbols, i.e.,

$$\hat{\epsilon}_0 = \underset{\epsilon}{\text{argmin}} \left\{ \sum_{\mu=1,2} |\mathbf{E}^{(\mu)} \bar{\mathbf{Y}}^{(\mu)}(\epsilon)|^2 \right\}. \tag{12}$$

Then, an estimate of the noise variance σ_z^2 in Eq. (8) can be computed as the average energy on the null symbols after CFO compensation. Moreover, based on Eqs. (10) and (11), the channel impulse response (CIR) estimates corresponding to the two transmit elements, i.e., $\hat{\mathbf{h}}^{(\mu)} = [\hat{h}_0^{(\mu)}, \hat{h}_1^{(\mu)}, \dots, \hat{h}_L^{(\mu)}]^T$, $\mu = 1, 2$, can be given by

$$\hat{\mathbf{h}}^{(\mu)} = [\mathbf{D}^{(\mu)} \mathbf{G}^{(\mu)}]^\dagger \bar{\mathbf{Y}}^{(\mu)}, \tag{13}$$

and thus the DFR submatrix estimates are $\hat{\mathbf{H}}_n^{(\mu)} = \mathbf{G}_n \hat{\mathbf{h}}^{(\mu)}$, $n = 0, \dots, N - 1$, where we have defined $\bar{\mathbf{Y}}^{(\mu)} = \bar{\mathbf{Y}}^{(\mu)}(\hat{\epsilon}_0)$, $\mathbf{D}^{(\mu)} = \text{diag}\{\mathbf{d}^{(\mu)}\}$, $\mathbf{G}^{(1)} = [\mathbf{G}_{2p_1}^T, \mathbf{G}_{2p_2}^T, \dots, \mathbf{G}_{2p_Q}^T]^T$, and $\mathbf{G}^{(2)} = [\mathbf{G}_{2p_1+1}^T, \mathbf{G}_{2p_2+1}^T, \dots, \mathbf{G}_{2p_Q+1}^T]^T$ with

$$\mathbf{G}_n = \begin{bmatrix} 1 & e^{-j(2\pi n/K)} & \dots & e^{-j(2\pi Ln/K)} \\ 1 & e^{-j[2\pi(n+N)/K]} & \dots & e^{-j[2\pi L(n+N)/K]} \\ \vdots & \vdots & \ddots & \vdots \\ 1 & e^{-j[2\pi(n+(M-1)N)/K]} & \dots & e^{-j[2\pi L(n+(M-1)N)/K]} \end{bmatrix}. \tag{14}$$

Remarks: It is worth mentioning that, different from the single-pilot-vector method adopted in Refs. 9,10, we here use Q vectors for the estimation of each channel in the SFBC-OSDM system. By such modification, the vector size restriction is relaxed from $M \geq L + 1$ to $M \geq (I + L + 1)/Q$, and thus more flexibility in the system configuration is obtained. Moreover, since M is chosen in practice as a power of 2 to allow DFT computations using the fast Fourier transform algorithm, a smaller M value can usually enable a reduction in the pilot overhead.

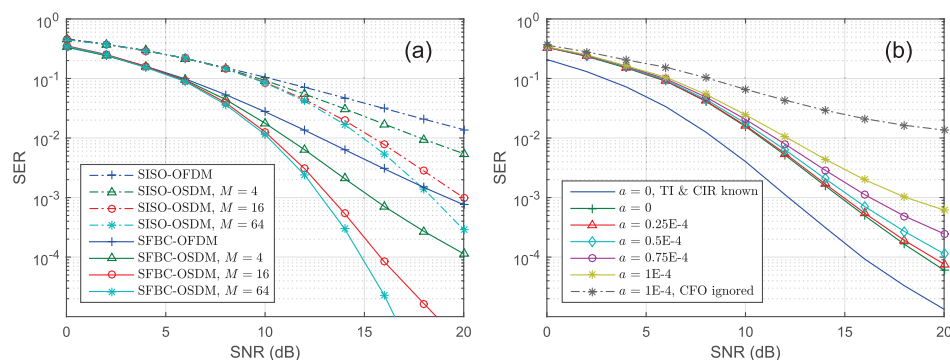


Fig. 1. (Color online) Simulation results. (a) Performance comparison among SISO/SFBC OFDM and OSDM systems with $a = 0.5 \times 10^{-4}$; (b) performance comparison among SFBC-OSDM systems with $M = 4$.

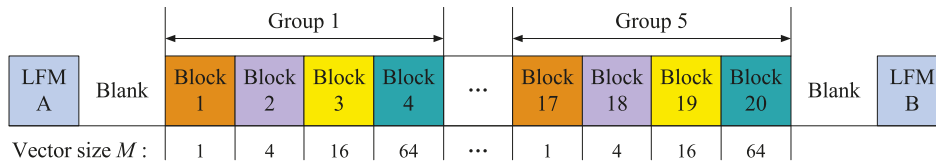


Fig. 2. (Color online) Packet structure used in the field experiment.

4. Simulation and experimental results

In this section, simulation and experimental results are provided to illustrate the uncoded SER performance of the proposed SFBC-OSDM system. We focus on data blocks of $K=1024$ quaternary phase-shift-keyed symbols with a duration of 256 ms, and the carrier frequency used here is 6 kHz. Four symbol vector sizes $M=1$ (equivalent to SFBC-OFDM), 4, 16, and 64 are considered, while the number of the VPs is, respectively, set to $Q=128, 32, 8,$ and 2 for channel estimation. Moreover, $I=16$ null symbols are arranged in each pilot sequence for CFO compensation. In simulation, the channel has identically and independently complex Gaussian distributed taps with memory $L=32$. It is easy to verify that the inequality $I+L+1 \leq MQ=128$ holds. For experimental data processing, we assume $L=64$, which corresponds to a channel delay spread of 16.25 ms. The interference induced by the CIR tail beyond this spread is treated as noise.

Figure 1 shows the simulation results, where the channel time variation is embodied by a constant Doppler scaling factor $a=v/c$ with v being the relative velocity between the transceiver pair and c denoting the sound speed in water (nominally 1500 m/s). Specifically, we fix $a=0.5 \times 10^{-4}$ in Fig. 1(a). As expected, the SFBC-OSDM system outperforms its SISO counterpart significantly. Besides the achieved spatial diversity, it can also be seen that, with the aid of CFO compensation, the SFBC-OSDM system obtains frequency diversity implicitly within each symbol vector. As M increases, more diversity gain is achieved and the SER performance improves accordingly. Furthermore, in Fig. 1(b), we fix $M=4$ and change the Doppler scaling factor $a \in [0,1] \times 10^{-4}$. Two scenarios are included as benchmarks: (1) time-invariant channel (i.e., $a=0$) with perfect CIR knowledge, and (2) time-variant channel ($a=1 \times 10^{-4}$) without CFO compensation. It is easy to observe that, compared to the CFO-ignorant processing, the null-symbol-based CFO compensation can effectively reduce the performance gap with the time-invariant channel case.

A field experiment was also conducted to evaluate the performance of the proposed SFBC-OSDM system in July 2016 at the Danjiangkou reservoir, Henan Province, China. The water depth was about 30–50 m. Two transducers were suspended at 10 and 15 m from a surface ship, and a single-element hydrophone was deployed at a depth of 20 m from an anchored ship. A total of 256 SFBC-OSDM packets were transmitted over 1 km. The packet structure is shown in Fig. 2, where two linear frequency-modulated (LFM) signal segments are used to provide a coarse estimate of the Doppler scaling factor for front-end resampling. Moreover, blocks with $M=1, 4, 16,$ and 64 are organized in an interleaved pattern, and thus we can approximately consider that the transmissions for all M values were under the same channel condition. Figures 3(a) and 3(b) display the normalized amplitude of the CIR estimates $|\hat{\mathbf{h}}^{(\mu)}|$ at block 1 in packet 1, and the maximum CFO estimate $\max|\hat{\epsilon}_0|$ (after resampling) in each packet, respectively. Our CFO search range is $[-2, 2]$ Hz and the

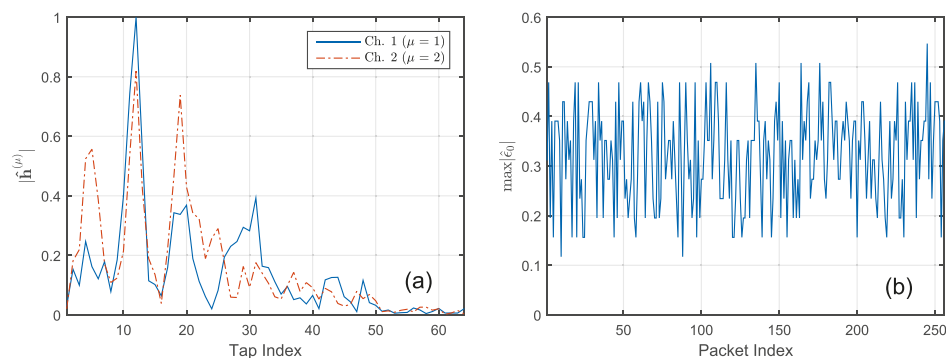


Fig. 3. (Color online) Experimental channel estimation results. (a) Normalized CIR amplitude; (b) maximum CFO estimate.

Table 1. Experimental SER performance of the SFBC-OSDM system.

	SFBC-OFDM	SFBC-OSDM		
	$M=1$	$M=4$	$M=16$	$M=64$
w/out CFO comp.	9.36×10^{-3}	3.94×10^{-3}	2.29×10^{-3}	2.09×10^{-3}
with CFO comp.	6.73×10^{-3}	1.97×10^{-3}	5.31×10^{-4}	3.40×10^{-4}

resulting values of $\max|\hat{\epsilon}_0|$ are all below 0.6 Hz (corresponding to $a = 1 \times 10^{-4}$ for carrier 6 kHz). Table 1 summarizes the experimental SER results of the SFBC-OSDM system with and without CFO compensation, from which the same observations as those in the simulation can be readily obtained.

5. Conclusions

We have proposed an SFBC-OSDM scheme for time-varying UWA channels, in which the post-resampling time variation is first mitigated by using null-symbol-based CFO compensation, and then CIR estimates are obtained by using precoded pilot vectors. Based on that, the proposed phase-rotation space-frequency decoding and equalization can achieve both spatial and frequency diversity gains, which make it outperform conventional SFBC-OFDM.

Acknowledgments

This work was supported by National Natural Science Foundation of China under Grant Nos. 61001153, 61401499, 61531015, and 61501374, and Natural Science Basic Research Plan in Shaanxi Province of China under Grant No. 2015JQ6220.

References and links

- ¹S. Zhou and Z. Wang, *OFDM for Underwater Acoustic Communications* (John Wiley & Sons, New York, 2014).
- ²J. Huang, S. Zhou, and P. Willett, "Nonbinary LDPC coding for multicarrier underwater acoustic communication," *IEEE J. Sel. Areas Commun.* **26**, 1684–1696 (2008).
- ³B. Li, S. Zhou, M. Stojanovic, L. Freitag, and P. Willett, "Multicarrier communication over underwater acoustic channels with nonuniform Doppler shifts," *IEEE J. Ocean. Eng.* **33**, 198–209 (2008).
- ⁴T. Kang, H. C. Song, and W. S. Hodgkiss, "Long-range multi-carrier acoustic communications in shallow water based on iterative sparse channel estimation," *J. Acoust. Soc. Amer.* **128**, EL372–EL377 (2010).
- ⁵B. Li and M. Stojanovic, "A simple design for joint channel estimation and data detection in an Alamouti OFDM system," in *Proceedings of MTS/IEEE OCEANS Conference*, Seattle, WA (2010), pp. 1–5.
- ⁶E. V. Zorita and M. Stojanovic, "Space-frequency block coding for underwater acoustic communications," *IEEE J. Ocean. Eng.* **40**, 303–314 (2015).
- ⁷J. Han and G. Leus, "Space-time and space-frequency block coded vector OFDM modulation," *IEEE Commun. Lett.* **21**, 204–207 (2017).
- ⁸X.-G. Xia, "Precoded and vector OFDM robust to channel spectral nulls and with reduced cyclic prefix length in single transmit antenna systems," *IEEE Trans. Commun.* **49**, 1363–1374 (2001).
- ⁹T. Ebihara and K. Mizutani, "Underwater acoustic communication with an orthogonal signal division multiplexing scheme in doubly spread channels," *IEEE J. Ocean. Eng.* **39**, 47–58 (2014).
- ¹⁰T. Ebihara and G. Leus, "Doppler-resilient orthogonal signal-division multiplexing for underwater acoustic communication," *IEEE J. Ocean. Eng.* **41**, 408–427 (2016).